Journal of Solid State Chemistry 184 (2011) 2131–2138

Contents lists available at ScienceDirect

Journal of Solid State Chemistry

journal homepage: www.elsevier.com/locate/jssc

Electronic band structure and optical properties of titanium oxyphosphates $Li_{0.50}Co_{0.25}TiO(PO_4)$ single crystals: An *ab-initio* calculations

Ali Hussain Reshak [a,b,*], H. Kamarudin [b], I.V. Kityk [c,e], R. Khenata [d,e], S. Auluck [f]

[a] Institute of Physical Biology-South Bohemia University, Nove Hrady 37333, Czech Republic
[b] School of Material Engineering, Malaysia University of Perlis, P.O Box 77, d/a Pejabat Pos Besar, 01007 Kangar, Perlis, Malaysia
[c] Electrical Engineering Department, Technical University of Czestochowa, Al.Armii Krajowej 17/19, Czestochowa, Poland
[d] Laboratoire de Physique Quantique et de Modélisation Mathématique de la Matière (LPQ3M), Université de Mascara, Mascara 29000, Algérie
[e] Department of Physics and Astronomy, King Saud University, P.O Box 2455, Riyadh 11451, Saudi Arabia
[f] National Physical Laboratory Dr. K S Krishnan Marg, New Delhi 110012, India

ARTICLE INFO

Article history:
Received 20 December 2010
Received in revised form
5 June 2011
Accepted 12 June 2011
Available online 21 June 2011

Keywords:
Structural properties
Band structure calculations
Optical properties
$Li_{0.50}Co_{0.25}TiO(PO_4)$
DFT
FP-LAPW

ABSTRACT

From the refined atomic positions obtained by Belmal et al. (2004) [1] using X-ray diffraction for $Li_{0.50}Co_{0.25}TiO(PO_4)$, we have performed a structural optimization by minimizing the forces acting on the atoms keeping the lattice parameters fixed at the experimental values. With this relaxed (optimized) geometry we have performed a comprehensive theoretical study of electronic properties and dispersion of the linear optical susceptibilities using the full potential linear augmented plane wave (FP-LAPW) method. The generalized gradient approximation (GGA) exchange-correlation potential was applied. In addition, the Engel-Vosko generalized gradient approximation (EVGGA) was used for comparison with GGA because it is known that EVGGA approach yields better band splitting compared to the GGA. We have calculated the band structure, and the total and partial densities of states. The electron charge densities and the bonding properties were analyzed and discussed. The complex dielectric optical susceptibilities were discussed in detail.

1. Introduction

Titanium oxyphosphates $M^{I}TiO(PO_4)$ (M^{I}=Li, Na, K, Rb, Cs, and Tl) have been extensively studied for their structural, linear, nonlinear optical, and electro-optical properties [2–8]. Belmal et al. [1] have studied the effect of substitution of a monovalent ion by a divalent ion. They found that this substitution leads to a new series of titanium oxyphosphates. For example the powder of $Li_{0.50}Co_{0.25}TiO(PO_4)$ was obtained from a stoichiometric mixture of Li_2CO_3, CoO, TiO_2, and $(NH_4)HPO_4$ heated at 300, 600, 800, and 1000 °C, respectively with intermediate regrinding. The final product is pink colored and the diffraction data were obtained at room temperature on a Philips PW 3040(θ–θ) diffractometer using a graphite monochromator [1]. Titanium oxyphosphate is used as active material for lithium batteries. Belharouak and Amine [9] have studied $Ni_{0.5}TiOPO_4$ oxyphosphate in the (NiO–TiO_2–P_2O_5) ternary diagram as a novel insertion compound for lithium batteries. The three-dimensional structure of this material consists of corner sharing octahedral [TiO_6], isolated [PO_4] tetrahedral, and [NiO_6] octahedral located between the titanium chains. The material also contains octahedral vacant sites that constitute favorable sites for lithium insertion. Kaoua et al. [10] have extended their research interest on titanium oxyphosphates ($M^{II}(TiO)_2(PO_4)_2$, with M^{II}=Mg, Fe, Co, Ni, Cu, and Zn) to vanadium oxyphosphates $M^{II}(V^{IV}O)_2(PO_4)_2$ (M^{II}=Co and Ni). They found that for each compound two phases were synthesized and characterized at room temperature. The structures consist of a three-dimensional framework built up of infinite chains of tilted corner-sharing [VO_6] octahedral, cross-linked by corner-sharing [PO_4] tetrahedral. Benmokhtar et al. [11] have synthesized and characterized a new titanium oxyphosphate $Mg_{0.50}TiO(PO_4)$ by X-ray diffraction, ^{31}P MAS-NMR, Raman diffusion, infrared absorption, and diffuse reflectance spectroscopy. The structure of $Mg_{0.50}TiO(PO_4)$ consists of infinite chains of corner-shared [TiO_6] octahedra parallel to the *c*-axis, cross-linked by corner-shared [PO_4] tetrahedra. Kenza et al. [12] have synthesized and characterized carbon-coated $Li_{0.5}Ni_{0.25}TiOPO_4$/C composite by the co-precipitation method using polyethylene glycol as a carbon source. The 3D structure exhibits an open framework favorable to interaction reactions. This $Li_{0.5}Ni_{0.25}TiOPO_4$/C composite exhibits excellent electrochemical performance with good capacity retention for 50 cycles. Approximately 200 mAh/g could be reached at C, C/2, C/5, and C/20 rates in the 0.53 V potential ranges. El Bouari and El Jazouli [13] have prepared $Pb_{0.5}Ti_2(PO_4)_3$ powder from dilute solutions of $Pb(NO_3)_2$,$6H_2O$ (I), $(NH_4)_2HPO_4$(II), and $TiCl_4$ in ethanol (III). Benmokhtar et al. [14] have prepared and characterized two new phases of phosphates $Fe_{0.5}TiO(PO_4)$ and $Fe_{0.5}Ti_2(PO_4)$

* Corresponding author at: Institute of Physical Biology, South Bohemia University, Zamek 136, 37333 Nove Hrady, Czech Republic. Fax: +420 386 361231.
E-mail address: maalidph@yahoo.co.uk (A.H. Reshak).

0022-4596/$ - see front matter © 2011 Elsevier Inc. All rights reserved.
doi:10.1016/j.jssc.2011.06.010

by X-ray diffraction, Mossbauer spectroscopy, and magnetic measurements.

From the above mentioned it is clear that there is a dearth of theoretical work on titanium oxyphosphates $Li_{0.50}Co_{0.25}TiO(PO_4)$. We take $Li_{0.50}Co_{0.25}TiO(PO_4)$ as a model oxyphosphate and therefore feel that it may be interesting to study its electronic properties. It may be used as electro-optical devices and could be a good material for lithium batteries. Theoretical studies will be helpful in elucidating the relationship between the structure and the dispersion of optical susceptibilities. In the past *ab-initio* density functional theory (DFT) calculations have been extensively applied for the computations of structural and optical parameters. Further, the efficiency of the optical susceptibilities is inherently dependent upon the structural features. As a result, it would be valuable to probe and understand the structure and the optical properties in this class of materials. A detailed description of the structural and optical properties of titanium oxyphosphates $Li_{0.50}Co_{0.25}TiO(PO_4)$ using a DFT full potential method is very crucial and could give important insights into understanding the origin of the electronic properties, their relations with principal structural parameters, chemical bonds, and their relation with dispersion of linear optical constants.

The computational details are given in Section 2. Results and discussions are presented in Section 3 and the conclusions in Section 4.

2. Structural features and computational details

The titanium oxyphosphates crystallizes in the monoclinic structure space group *P*-1. The experimental lattice parameters and the atomic position were given by Belmal et al. [1]. The structure of the titanium oxyphosphates $Li_{0.50}Co_{0.25}TiO(PO_4)$ is similar to that of $Li_{0.50}Ni_{0.25}TiO(PO_4)$ [15]. It is formed by a three-dimensional framework of TiO_6 octahedra and PO_4 tetrahedra. PO_4 groups are isolated from each other and connected to TiO_6 octahedra at the corners. Each TiO_6 octahedron shares four corners of its basic unit with four PO_4 tetrahedra and the two other corners with two TiO_6. TiO_6 octahedra form infinite chains Ti–O–Ti–O parallel to the **c**-axis. In these chains, a very short Ti–O bond and a very long one are alternating. Lithium atoms fully occupy the site 2*a*, whereas cobalt atoms occupy statistically half of the site 2*b*. The cobalt and lithium octahedrals form infinite chains of edge-sharing octahedral running parallel to the **a**-axis. Each TiO_6 shares two adjacent faces with LiO_6 and CoO_6 [1].

As mentioned above experiments show that this compound has a crystal structure corresponding to monoclinic symmetry and space group *P*21/*c*. In the experimental paper it is mentioned that Co atoms have a fractional occupancy 0.5. As the Wien2k code does not handle fractional occupancies, we have chosen to do the calculations using a supercell corresponding to triclinic symmetry and spacegroup *P*-1. We have optimized the structure by minimization of the forces (1 mRy/a.u.) acting on the atoms, keeping the lattice parameters fixed at the experimental values. From the relaxed geometry the electronic structure and the chemical bonding can be determined and various spectroscopies can be simulated and compared with experimental data. Once the forces are minimized in this construction one can then find the self-consistent density at these positions by turning off the relaxations and driving the system to self-consistency. The optimized atomic positions are presented in Table 1.

Self-consistent calculations of the electronic structure and optical properties based on the scalar relativistic full-potential linearized augmented plane wave (FP-LAPW) method were carried out using the WIEN2K package [16]. This is a very precise and efficient approach to solve the Kohn–Sham equation within a framework of DFT. Within a framework of this approach, the potential and corresponding charge density is expanded into lattice harmonics inside each atomic sphere and as a Fourier series in the interstitial region. The exchange correlation potential was treated using two approximations: the generalized gradient approximation (GGA) [17] for the total energy calculations and the Engel–Vosko GGA (EVGGA) formalism [18] for band structure calculations. It is well known that in the self-consistent band structure calculation within the DFT approach, the generalized gradient approximation GGA approach is based on simple model assumptions, which are not sufficiently flexible to accurately reproduce the exchange correlation energy and its charge space derivative. Engel and Vosko [18] considered this shortcoming and constructed a new functional form of GGA, which is able to reproduce better exchange potential at the expense of less agreement in the exchange energy by taking into account the inter-particle interactions. This approach (EVGGA) yields better band splitting compared to the GGA [18].

Table 1
The optimized atomic positions.

Atom	*x* (optimized)	*y* (optimized)	*z* (optimized)
Li	0.00000	0.00000	0.00000
Li	0.00000	0.50000	0.50000
Co	0.50000	0.00000	0.00000
Ti	0.73677	0.22967	0.34113
Ti	0.25294	0.71942	0.16789
P	0.24457	0.12867	0.37592
P	0.75444	0.63073	0.11844
O	0.71624	0.14511	0.11191
O	0.23310	0.66370	0.39109
O	0.74970	0.99939	0.79671
O	0.23701	0.49554	0.71478
O	0.27062	0.48119	0.05847
O	0.76166	0.98876	0.45008
O	0.43482	0.23171	0.86536
O	0.55817	0.75050	0.62099
O	0.95244	0.75220	0.10477
O	0.05177	0.25448	0.64021

The Kohn–Sham equations are solved using a basis function of linear APW's. To achieve energy eigenvalues convergence, the wave functions in the interstitial regions were expanded in plane waves with a cut-off $K_{max}=9/R_{MT}$, where R_{MT} denotes the smallest atomic sphere radius and K_{max} gives the magnitude of the largest *K* vector in the plane wave expansion. The muffin-tin (MT) radii were assumed to be 1.87 atomic units (a.u.) for Li, 1.91 a.u. for Co, 1.7 a.u. for Ti, and 1.44 a.u. for O and P atoms. The valence wave functions inside the MT were expanded up to $l_{max}=10$ while the charge density was Fourier expanded up to $G_{max}=14$ (a.u)$^{-1}$. The self-consistency was achieved using 300 **k**-points in the irreducible Brillouin zone (IBZ). The linear optical susceptibilities were calculated using summation over 500 **k**-points within the IBZ. The self-consistent calculations are converged since the total energy of the system is stable within 10^{-5} Ry.

Since $Li_{0.50}Co_{0.25}TiO(PO_4)$ crystallizes in the monoclinic structure space group *P*-1, the dielectric tensor has three principal components corresponding to the electric field $\vec{E}$ directed along **a**, **b**, and **c**-crystallographic axes. These are the complex tensor components; $\varepsilon^{xx}(\omega)$, $\varepsilon^{yy}(\omega)$, and $\varepsilon^{zz}(\omega)$. The imaginary part of these three complex components are $\varepsilon_2^{xx}(\omega)$, $\varepsilon_2^{yy}(\omega)$, and $\varepsilon_2^{zz}(\omega)$, respectively. The inter-band transitions of the dielectric function $\varepsilon(\omega)$ are usually presented as a superposition of direct and indirect transitions. We can neglect the indirect inter-band transitions formed by elecron–phonon interactions that are expected to give a small contribution to $\varepsilon(\omega)$ [19]. To calculate the direct inter-band contributions to the imaginary part of the dielectric function $\varepsilon_2(\omega)$, it is necessary to perform summation over all possible transitions from the occupied to the unoccupied band states. Taking the appropriate inter-band transition matrix elements into account, as the investigated compound is metallic we must

include the Drude term (intra-band transitions) [20]:

$$\varepsilon_2(\omega) = \varepsilon_{2\text{inter}}(\omega) + \varepsilon_{2\text{intra}}(\omega) \quad (1)$$

where

$$\varepsilon_{2\text{intra}}(\omega) = \frac{\omega_P \tau}{\omega(1+\omega^2\tau^2)} \quad (2)$$

where ω_P is the anisotropic plasma frequency [21] and τ is the mean free time between collisions:

$$\omega_P^2 = \frac{8\pi}{3}\sum_{kn} \vartheta_{kn}^2 \delta(\varepsilon_{kn}) \quad (3)$$

where ε_{kn} is $E_n(k) - E_F$ and ϑ_{kn} is the electron velocity (in basal plane) squared.

3. Results and discussion

3.1. Band structure and density of states

We present the band structure, and total and partial density of states (DOS) using GGA and EVGGA in Figs. 1 and 2. Following these figures one can compare GGA and EVGGA. It is clear that using EVGGA causes a shift in the structures from −20.0 to 5.0 eV by 0.5 eV towards lower energies with respect to the structures in GGA, while it shifts the structures from 5.0 eV and above by 0.5 eV towards higher energies. We should emphasize that using EVGGA the Fermi energy (E_F) is situated at 0.602 eV, while with GGA it is situated at 0.545 eV. That is clear the EVGGA cause to shift the E_F towards lower energy by around 0.057 eV resulting in a DOS at E_F–$N(E_F)$=3.0 states/Ry cell for GGA and 2.66 states/Ry cell for EVGGA. For this reason we show all the results for EVGGA approach. These figures suggest that the band structure and the DOS can be divided into six distinct spectral groups/structures. We have enlarged the band structure near E_F in order to show the overlapping of the bands around E_F. We find that Co-*d* and Ti-*d* states determine the overlapping around E_F with small admixture of Ti-*s*/*p*, P-*s*/*p*, and O-*s*/*p* states. The DOS at Fermi energy (E_F) is determined by the overlap between the valence and the conduction bands; this overlap is strong indicating metallic behavior. Although, the dispersions of the band structure and DOS obtained within GGA and EVGGA are very similar in the matter of groups/structures, there are some minor differences that can lead to different electronic properties. The electronic specific heat coefficient (γ), which is a function of density of states, can be calculated using the expression:

$$\gamma = \tfrac{1}{3}\pi^2 N(E_F) k_B^2 \quad (4)$$

where $N(E_F)$ is the density of states at Fermi energy E_F, and k_B is the Boltzmann constant. The calculated density of states at Fermi energy $N(E_F)$ enables us to calculate the bare electronic specific heat coefficient, which is found to be 0.52 mJ/mol K^2 for GGA and

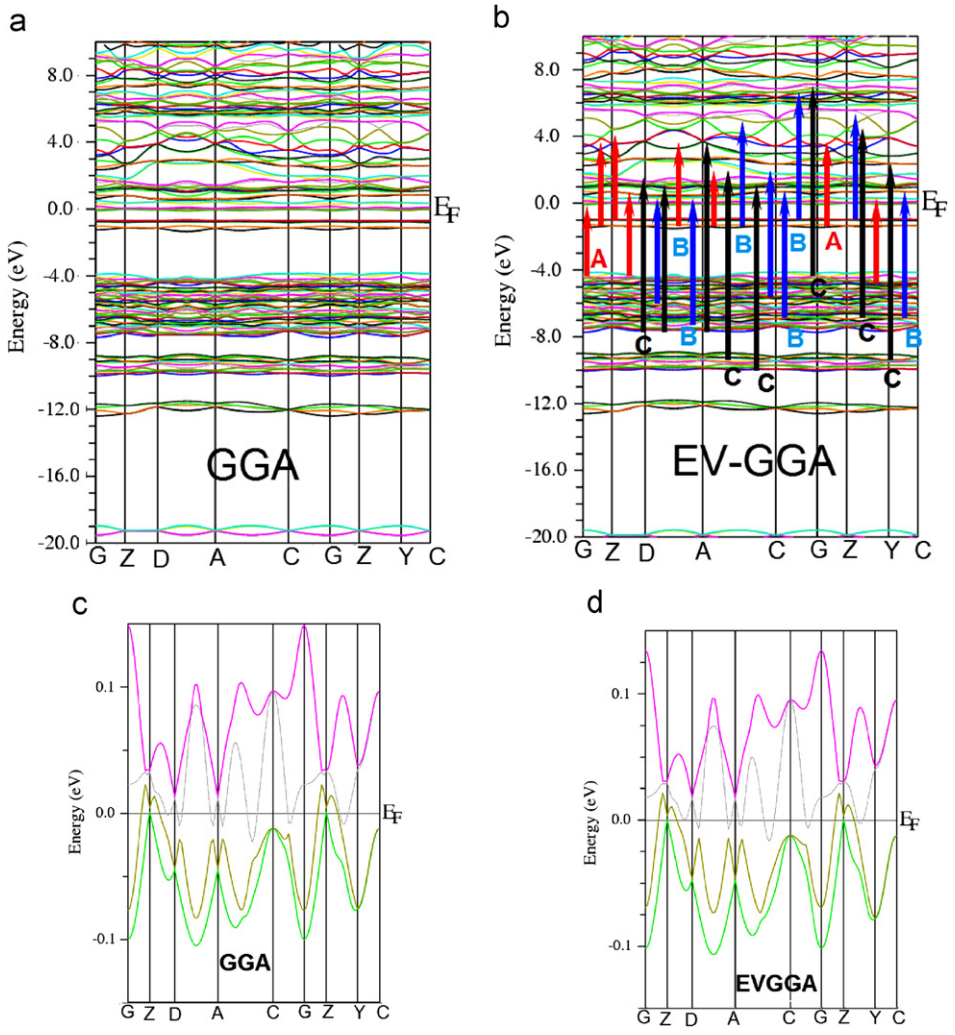

Fig. 1. The calculated band structure (a) GGA, (b) EVGGA with the optical transitions depicted on a generic band structure, (c) enlarged GGA band structure to show the overlapped bands around Fermi level, and (d) enlarged EVGGA band structure to show the overlapped bands around Fermi level.

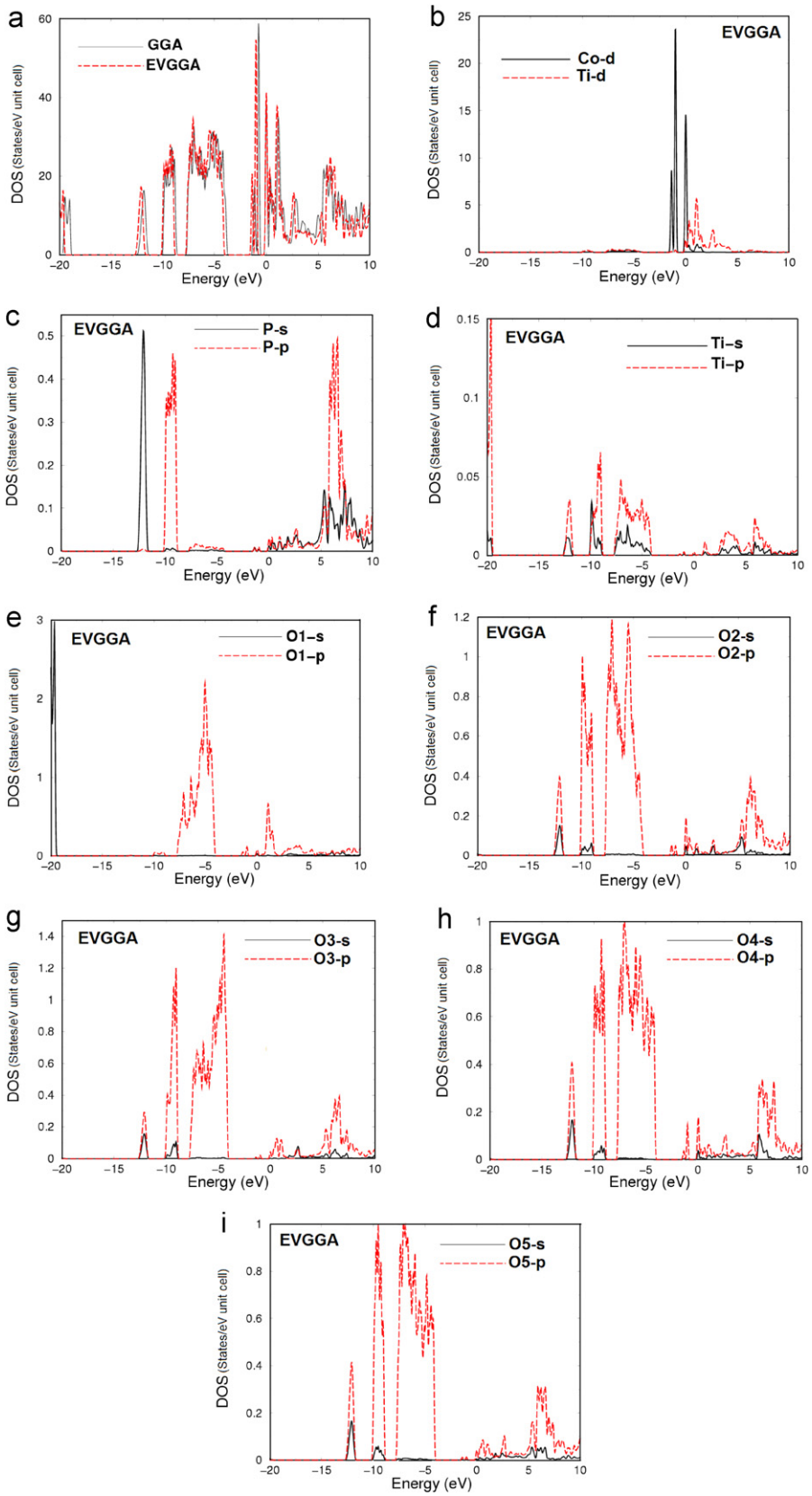

Fig. 2. (a) Calculated total density of states (states/eV unit cell) using GGA (**dark solid curve**) and EVGGA (light dashed curve), and (b–i) calculated partial densities of states (states/eV unit cell) using EVGGA.

0.46 mJ/mol K^2 for EVGGA. We hope that future experiments will help in determining which of the approximations (GGA or EVGGA) is more suitable.

From the PDOS (see Fig. 2b–i) we are able to identify the angular momentum character of the various structures. The lowest group (first group), which is located at −20.0 eV, is originating

mainly from Ti-*s*/*p* and O1-*s* states. The second group (−12.0 eV) arises from P-*p*, Ti-*s*/*p*, and O2-5*s*/*p* states. The third group (−10.0 eV) is a mixture of P-*s*/*p*, Ti-*s*/*p*, O1*p*, and O2-5*s*/*p* states. The fourth group (−8.0 to −4.0 eV) is a mixture of P-*p*, Ti-*s*/*p*, and O1-5*p* states. The group from −2.0 eV up to Fermi energy is formed by Co-*d* and O1-5*p* states. The group around Fermi energy consists of Co-*d*, Ti-*s*/*p*/*d*, P-*s*/*p*, and O1-5*s*/*p* states. The last group from Fermi energy and above is hybridization of Co-*d*, Ti-*s*/*p*/*d*, P-*s*/*p*, and O1-5*s*/*p* states. From the PDOS, we may note that there is a strong hybridization between various states. P-*s* and P-*p* are hybridized strongly within the energy range from Fermi energy up to 6.0 eV. The energies around −12.0 eV and above between 2.0 and 5.0 eV O2-5*s* are hybridized with O2-5*p*.

The origin of the chemical bonding can be elucidated from the total and the partial densities of states. We find that the densities of states, extending from −10.0 eV up to Fermi energy (E_F), are mainly originated from Co-*d* states (24.0 electrons/eV), Ti-*s* states (0.04 electrons/eV), Ti-*p* states (0.06 electrons/eV), O1-*p* states (2.2 electrons/eV), O2-5-*p* states (1.2 electrons/eV), and O2-5-*s* states (0.1 electrons/eV). This is obtained by comparing the total densities of states with the angular momentum projected densities of states of Co-*d*, Ti-*s*/*p*, O1*p*, O2-5*p*, and O2-5*sp* states as shown in Fig. 2. These results show that some electrons from Co-*d*, O-*s*/*p*, and Ti-*s*/*p* states were transferred into valence bands (VBs) and contribute to weak covalence interactions between O–O, Ti–Ti, and Co–Co atoms, and substantial covalence interactions between Co and O, Co and Ti, and Ti and O atoms. Accordingly, we can also say that the covalent strength of Co–O, Co–Ti, and Ti–O bonds is weaker than that of O–O, Co–Co, and Ti–Ti bonds.

To explain the bonding properties of $Li_{0.50}Co_{0.25}TiO(PO_4)$ we have plotted the electronic charge density contour in the (011) plane shown in Fig. 3a. The contour plot shows more ionic and partial covalent bonding between Li and O, which depends on Pauling electro-negativity difference of Li (0.93) and O (2.58) atoms. As a result, we observe a large Li electronic charge transferred to O site. This can be seen easily by color charge density scale, where blue color (+0.5000) corresponds to the maximum charge accumulation site. The interaction between Co and O produces covalent-like bond due to small electro-negativity difference around 0.7 (electro-negativity of Co is 1.88) and also due to the hybridized Co-3*d* states with O-*p* states. Also the electronic charge density between Ti(1.54) and O shows more strong covalent bonding. As the electro-negativity of P (2.19) is close to the O (2.58) and difference between there electro-negativity is small as 0.39, this may cause very strong covalent bonding with respect to Co–O, Li–O, or Ti–O. Another reason for this strong covalent bonding is that P is tetrahedrally coordinated by four O ions (see Fig. 3b). The angle between O–P–O is 111.56^0 and bond lengths between P–O and O–O are 1.5752 and 2.6 Å, respectively. Due to this strong hybridization the *d*-states of P and *p*-states of O cause the crystal field splitting of *d*-states of P also. This was explained in detail in the part discussing the density of states data. From the relaxed geometry we have calculated the bond lengths and the bond angles. The calculated bond lengths and the bond angles were compared with the experimental data [1] and good agreement was found (see Tables 2 and 3).

3.2. Fermi surface

In condensed matter physics, the Fermi surface is useful for predicting the thermal, electrical, magnetic, and optical properties of metals, semimetals, and doped semiconductors. The Fermi surface separates the unfilled orbitals from the filled orbitals, at absolute zero. The Fermi level is determined via the Kohn–Sham eigenvalue of the highest occupied state. From the band structure plot in Fig. 1 it is clear that two bands cross the Fermi energy. Fig. 4a and b shows the Fermi surface of $Li_{0.50}Co_{0.25}TiO(PO_4)$, using GGA and EVGGA, respectively. Following these figures we should emphasize that the shape of Fermi surface obtained by EVGGA is different from that obtained by GGA. That is attributed to the fact that EVGGA approach yields better band splitting compared to the GGA, resulting in the density of states at E_F–$N(E_F)$ and bare electronic specific heat coefficient for GGA being less than that obtained by EVGGA.

3.3. First order (linear) optical susceptibility dispersion

Fig. 5a and b displays the variation of the imaginary (responsible for absorption) part of the electronic dielectric function $\varepsilon_2^{xx}(\omega)$, $\varepsilon_2^{yy}(\omega)$, and $\varepsilon_2^{zz}(\omega)$ for both GGA and EVGGA. The broadening due to electron–phonon interactions was taken to be 0.1 eV so as bring out all the structures [22]. Following $\varepsilon_2^{xx}(\omega)$, $\varepsilon_2^{yy}(\omega)$, and $\varepsilon_2^{zz}(\omega)$ spectra one can see that EVGGA produces better band

Table 2
Our calculated bond lengths in comparison with experimental data [1].

Bond length (Å)	Exp.	This work	Bond length (Å)	Exp.	This work
Li–O(1)	2.11(1)	2.10	Ti–O(1′)	2.26(1)	2.27
Li–O(1′)	2.11(1)	2.10	Ti–O(2)	2.03(3)	2.03
Li–O(2)	2.25(2)	2.23	Ti–O(3)	1.88(1)	1.87
Li–O(5)	2.11(1)	2.12	Ti–O(4)	1.99(1)	2.00
Co–O(1)	2.14(2)	2.15	Ti–O(5)	1.86(2)	1.85
Co–O(1′)	2.14(2)	2.15	P–O(2)	1.58(1)	1.57
Co–O(2)	2.13(3)	2.12	P–O(3)	1.56(2)	1.55
Co–O(4)	2.07(1)	2.06	P–O(4)	1.56(3)	1.55
Co–O(4)	2.07(1)	2.06	P–O(5)	1.57(2)	1.56
Ti–O(1)	1.68(2)	1.66			

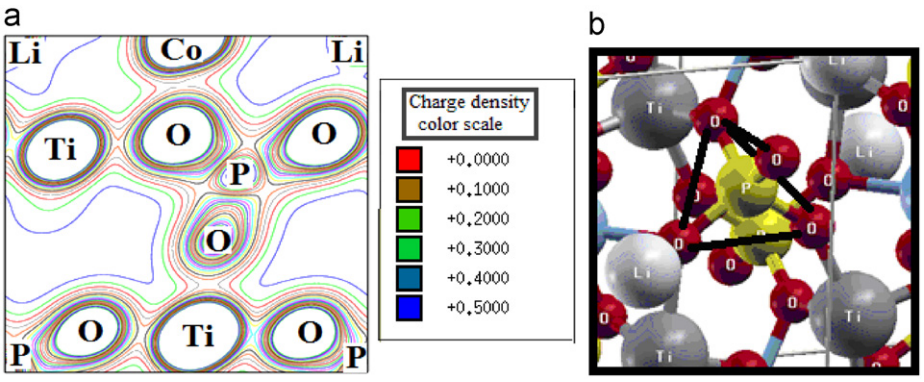

Fig. 3. (a) Total valence charge densities in the (0 1 1) plane, and (b) shows that P is tetrahedrally coordinated by four O ions. (For interpretation of the references to color in this figure legend, the reader is referred to the web version of this article.)

splitting, which may result in correct optical transitions between the occupied and unoccupied bands. For this reason we present all the results for EVGGA. To the best of our knowledge, there is no experimental data or theoretical calculations are available in the literatures for the optical properties of the investigated compound to compare with our results. But we can refer to our previous work [23] in which we compared our calculated optical properties with the measured one to justify the reliability of the DFT methodology for the calculation of dielectric functions.

Following Fig. 4b, one can see that all the structures are shifted towards higher energies by around 0.5 eV with higher magnitude especially for the first spectral structure at lower energies. Also we note that all components $\varepsilon_2^{xx}(\omega)$, $\varepsilon_2^{yy}(\omega)$, and $\varepsilon_2^{zz}(\omega)$ display two principal structures situated around 1.0 and 6.0 eV, respectively. Some insignificant humps are observed between these structures and in the tail of these three components. We should emphasize that there is a considerable anisotropy between the three components. At energies 1.0 eV and between 3.0 and 7.0 eV the tensor component $\varepsilon_2^{zz}(\omega)$ is dominant and shows a larger contribution, whereas at middle and higher energies all the three polarizations give comparable contributions.

We have performed calculations of $\varepsilon_2^{xx}(\omega)$, $\varepsilon_2^{yy}(\omega)$, and $\varepsilon_2^{zz}(\omega)$ with and without the inclusion of the Drude term. The effect of the Drude term is significant for energies less than 1 eV. The sharp rise at low energies is due to the Drude term. The peaks in the optical response are caused by the allowed electric–dipole transitions between the valence and the conduction bands. In order to identify these structures we should consider the values of the optical matrix elements. The observed structures would correspond to those transitions that have large optical matrix dipole transition elements.

It would be worthwhile to attempt to identify the band transitions that are responsible for the spectral structures in $\varepsilon_2^{xx}(\omega)$, $\varepsilon_2^{yy}(\omega)$, and $\varepsilon_2^{zz}(\omega)$ using our calculated band structure. Fig. 1b presents the optical transitions that are responsible for the spectral structures in $\varepsilon_2^{xx}(\omega)$, $\varepsilon_2^{yy}(\omega)$, and $\varepsilon_2^{zz}(\omega)$. For simplicity we have labeled the transitions in Fig. 1b, as A, B, and C. The transitions A are responsible for the structures in $\varepsilon_2^{xx}(\omega)$, $\varepsilon_2^{yy}(\omega)$, and $\varepsilon_2^{zz}(\omega)$ for energies up to 4.0 eV, transitions B are responsible for the structures in the energy range 4.0–8.0 eV, and transitions C are responsible for the structures between 8.0 and 12.0 eV.

From the imaginary parts of the dielectric functions $\varepsilon_2^{xx}(\omega)$, $\varepsilon_2^{yy}(\omega)$, and $\varepsilon_2^{zz}(\omega)$ the real parts $\varepsilon_1^{xx}(\omega)$, $\varepsilon_1^{yy}(\omega)$, and $\varepsilon_1^{zz}(\omega)$ can be calculated using the Kramers–Kronig relations [24]. The $\varepsilon_1^{xx}(\omega)$, $\varepsilon_1^{yy}(\omega)$, and $\varepsilon_1^{zz}(\omega)$ are shown in Fig. 4c. Using the calculated dispersions of imaginary and real parts of the dielectric function one can evaluate other optical properties such as reflectivity spectra $R(\omega)$, absorption coefficients $I(\omega)$, refractive indices $n(\omega)$, loss function $L(\omega)$, and the conductivity $\sigma(\omega)$.

In Fig. 4d, we show the three components of the calculated reflectivity spectra. It is interesting that there is an abrupt reduction in the reflectivity spectrum at 12.5 eV confirming the occurrence of collective plasmon resonance excitations. The depth of the plasmon minimum is determined by the imaginary part of the dielectric function at the plasma resonance and is representative of the degree of overlap between the inter-band absorption regions.

Electron energy loss spectroscopy is a valuable tool for investigating various aspects of materials [25]. The plasmon losses corresponding to a collective oscillation of the valence electrons and their energies are related to the density of valence electrons. In the case of inter-band transitions, which consist mostly of plasmon excitations, the scattering probability for volume losses is directly connected to the energy loss function. In Fig. 4e, the energy loss function is plotted in basal-plane and in direction of ***c***-axis. There are other features in this spectrum, in

Table 3
Our calculated bond angles in comparison with experimental data [1].

Bond angle (°)	Exp.	This work	Bond angle (°)	Exp.	This work
O(1)–Li–O(1′)	180.0(1)	179.3	O(1′)–Ti–O(5)	81.7(3)	81.0
O(1)–Li–O(2)	72.8(3)	73.0	O(2)–Ti–O(5)	89.3(3)	90.0
O(1′)–Li–O(2)	107.2(1)	107.9	O(3)–Ti–O(5)	93.1(2)	92.8
O(1)–Li–O(2)	107.2(1)	107.9	O(4)–Ti–O(5)	160.5(3)	160.0
O(1′)–Li–O(2)	72.8(3)	73.3	O(1)–Co–O(1′)	180.0(1)	179.4
O(2)–Li–O(2)	180.0(1)	179.2	O(1)–Co–O(2)	74.6(2)	75.0
O(1)–Li–O(5)	100.2(2)	99.8	O(1′)–Co–O(2)	105.3(3)	106.0
O(1′)–Li–O(5)	79.7(3)	79.0	O(1)–Co–O(2)	105.3(3)	106.0
O(2)–Li–O(5)	102.2(1)	103.0	O(1′)–Co–O(2)	74.6(2)	74.0
O(2)–Li–O(5)	77.7(3)	77.1	O(2)–Co–O(2)	180.0(1)	179.0
O(1)–Li–O(5)	79.7(3)	80.0	O(1)–Co–O(4)	80.4(3)	80.0
O(1′)–Li–O(5)	100.2(2)	99.8	O(1′)–Co–O(4)	99.5(1)	99.0
O(2)–Li–O(5)	77.7(3)	77.1	O(2)–Co–O(4)	76.7(2)	77.0
O(2)–Li–O(5)	102.2(1)	103.0	O(2)–Co–O(4)	103.2(3)	104.0
O(5)-Li-O(5)	180.0(1)	179.6	O(1)–Co–O(4)	99.5(1)	99.0
O(1)–Ti–O(1′)	172.6(3)	172.0	O(1′)–Co–O(4)	80.4(3)	80.9
O(1)–Ti–O(2)	98.5(1)	98.0	O(2)–Co–O(4)	103.2(3)	103.0
O(1′)–Ti–O(2)	74.1(2)	73.7	O(2)–Co–O(4)	76.7(2)	77.0
O(1)–Ti–O(3)	99.9(2)	99.1	O(4)–Co–O(4)	180.0(1)	179.0
O(1′)–Ti–O(3)	87.2(2)	87.0	O(2)–P–O(3)	110.6(3)	110.9
O(2)–Ti–O(3)	160.6(4)	160.0	O(2)–P–O(4)	106.3(2)	107.0
O(1)–Ti–O(4)	98.5(2)	98.0	O(3)–P–O(4)	109.8(3)	110.0
O(1′)–Ti–O(4)	79.4(3)	80.0	O(2)–P–O(5)	110.3(2)	110.8
O(2)–Ti–O(4)	80.8(1)	81.0	O(3)–Li–O(5)	108.01(1)	109.0
O(3)–Ti–O(4)	90.8(1)	90.0	O(4)–Li–O(5)	111.5(2)	111.56
O(1)–Ti–O(5)	99.5(1)	100.0			

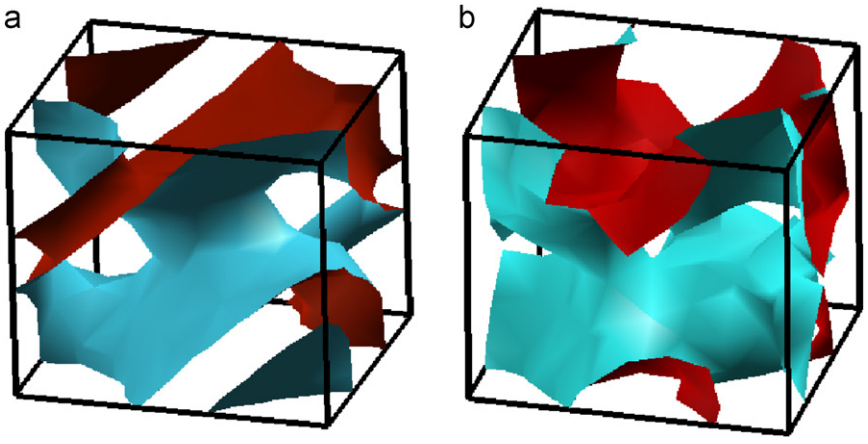

Fig. 4. (a) Fermi surface using GGA, (m) Fermi surface using EVGGA.

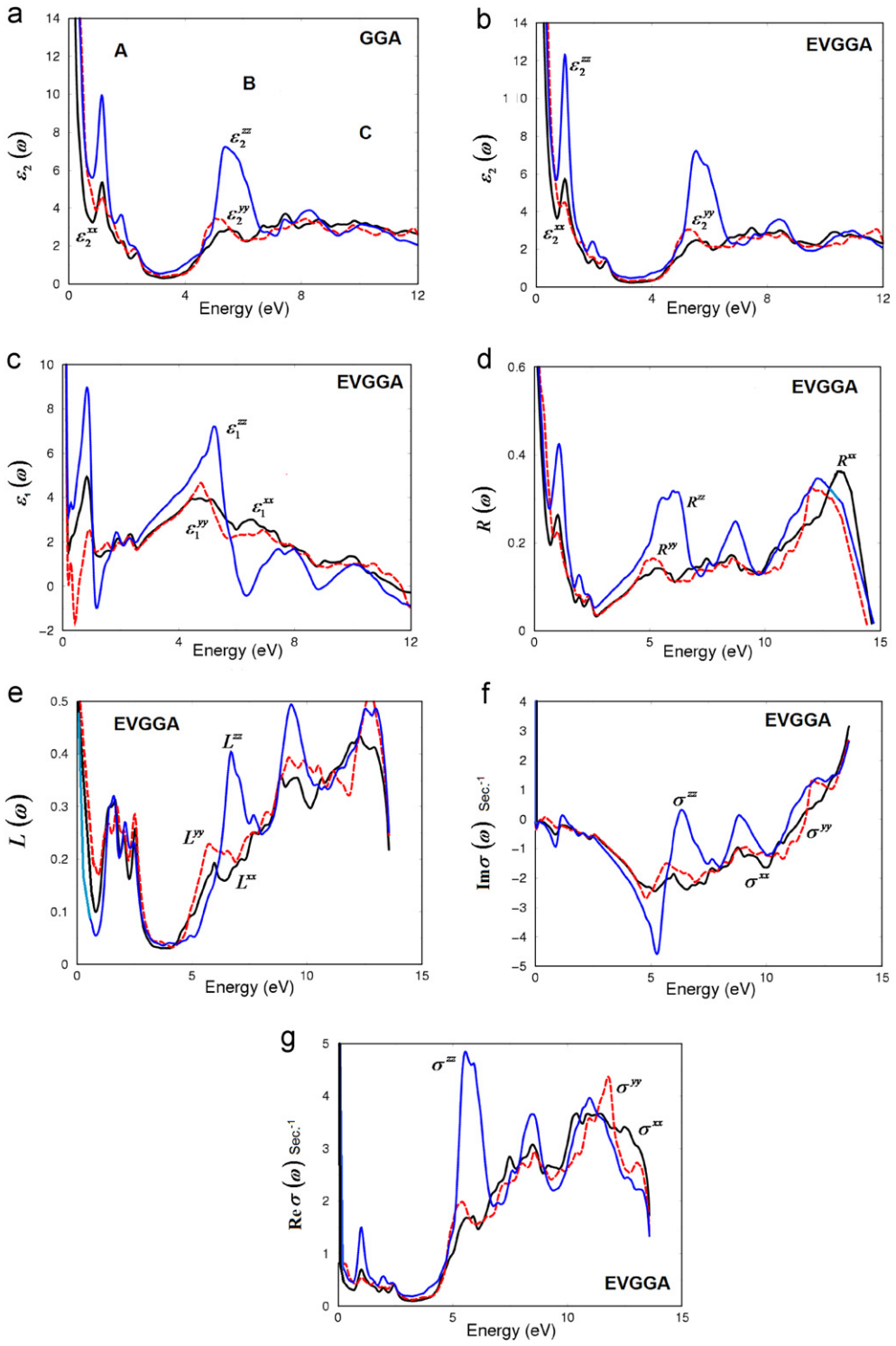

Fig. 5. Calculated $\varepsilon_2^{xx}(\omega)$ (**dark solid curve**—**black**), $\varepsilon_2^{yy}(\omega)$ (light dashed curve—red color online), and $\varepsilon_2^{zz}(\omega)$ (light solid curve—blue spectra: (a) GGA, (b) EVGGA, (c) calculated $\varepsilon_1^{xx}(\omega)$ (**dark solid curve**—**black**), $\varepsilon_1^{yy}(\omega)$ (light dashed curve—red color online), and $\varepsilon_1^{zz}(\omega)$ (light solid curve—blue color online) spectra using EVGGA; (d) calculated $R^{xx}(\omega)$ (**dark solid curve**—**black**), $R^{yy}(\omega)$ (light dashed curve—red color online), and $R^{zz}(\omega)$ (light solid curve—blue color online) spectra using EVGGA; (e) calculated loss function $L^{xx}(\omega)$ (**dark solid curve**—**black**), $L^{yy}(\omega)$ (light dashed curve—red color online), and $L^{zz}(\omega)$ (light solid curve—blue color online) spectra using EVGGA; (f) calculated imaginary part of the conductivity of $\sigma^{xx}(\omega)$ (**dark solid curve**—**black**), $\sigma^{yy}(\omega)$ (light dashed curve—red color online), and $\sigma^{zz}(\omega)$ (light solid curve—blue color online) spectra using EVGGA. The optical conductivity in 10^{15} s^{-1} (g) calculated real part of the conductivity of $\sigma^{xx}(\omega)$ (**dark solid curve**—**black**), $\sigma^{yy}(\omega)$ (light dashed curve—red color online), and $\sigma^{zz}(\omega)$ (light solid curve—blue color online) spectra using EVGGA. The optical conductivity in 10^{15} s^{-1}. (For interpretation of the references to color in this figure legend, the reader is referred to the web version of this article.)

addition to the plasmon peak, associated with inter-band transitions. The plasmon peak is usually the most intense feature in the spectrum and this is at energy where $\varepsilon_1(\omega)$ goes to zero. The energy of the maximum peak of $(-\varepsilon_1(\omega))^{-1}$ is observed at $\sim$12.5 eV for $L^{xx}(\omega)$, $L^{yy}(\omega)$, and $L^{zz}(\omega)$, which are assigned to the energy of volume plasmon $\hbar\omega_p$. The calculated optical conductivity dispersions Im$\sigma(\omega)$ and Re $\sigma(\omega)$ are shown in Fig. 4f and g. It also shows anisotropy between $\sigma^{xx}(\omega)$, $\sigma^{yy}(\omega)$, and $\sigma^{zz}(\omega)$.

The optical conductivity (OC) is related to the frequency-dependent dielectric function $\varepsilon(\omega)$ as $\varepsilon(\omega) = 1 + 4\pi i\sigma(\omega)/\omega$. The peaks in the optical conductivity spectra are determined by the electric–dipole transitions between the occupied band states of the unoccupied conduction states.

4. Conclusion

In the present work we have done an optimization of the refined crystal structure following X-ray powder diffraction data for $Li_{0.50}Co_{0.25}TiO(PO_4)$ single crystals. The obtained relaxed geometry was used to perform a comprehensive theoretical study of the structural properties and dispersion of the linear optical susceptibilities using the full potential linear augmented plane wave method within a framework of GGA and EVGGA approaches. Both the band structure and the density of states show that this compound is metallic with a DOS at E_F, $N(E_F)$ of 3.0 states/Ry cell using GGA, and 2.66 states/Ry cell using EVGGA. Although the band structure and DOS obtained within GGA and EVGGA are very similar, the principal groups/structures are spectrally shifted by around 0.5 eV towards the lower energies with respect to structure obtained by GGA. The bare electronic specific heat coefficient is found to be 0.52 mJ/mol K^2 for GGA and 0.46 mJ/mol K^2 for EVGGA. We have studied the electronic charge density contour in the (0 1 1) crystallographic plane to explain the bonding properties. The complex dielectric optical susceptibilities were analyzed and discussed in detail.

Acknowledgments

This work was supported from the Institutional Research Concept of the Institute of Physical Biology, UFB (No.MSM6007665808), the program RDI of the Czech Republic, the project CENAKVA (No. CZ.1.05/2.1.00/01.0024), the Grant no. 152/2010/Z of the Grant Agency of the University of South Bohemia, and the School of Material Engineering, Malaysia, University of Perlis, P.O Box 77, d/a Pejabat Pos Besar, 01007 Kangar, Perlis, Malaysia. The author (R. Kh.) extends his appreciation to the Deanship of Scientific Research at King Saud University for funding the work through the research group Project no. RGP-VPP-088.

References

[1] H. Belmal, A. El Jazouli, J.P. Chaminade, Phosphorus Res. Bull. 15 (2004) 131–135.
[2] R. Masse, J.C. Grenier, Bull. Soc. Franc. Mineral. Cristallogr 91 (1971) 437–439.
[3] R. Tordjman, Masse, J.C. Guitel, Z. Kristallogr. 139 (1974) 103–115.
[4] P.G. Nagornyi, A.A. Kapshuk, N.V. Stus, N.S. Slobodyanik, A.N. Chernega, Russ. J. Inorg. Chem. 36 (1991) 1551–1552.
[5] K.W. Godfrey, P.A. Thomas, B.E. Watts, Mater. Sci. Eng. B 9 (1991) 479–483.
[6] J.G. Robertson, J.M.S. Fletcher, Skakle, A.R. West, J. Solid State Chem. 109 (1994) 53–59.
[7] William T.A. Harrison, Thurman E. Gier, Galen D. Stucky, Arthur J. Schultz, Mater. Res. Bull. 30 (11) (1995) 1341–1349.
[8] M. Kunz, R. Dinnebier, L.K. Cheng, E.M. Mccarron, D.E. Cox, J.B. Parise, M. Gehrke, J. Calabrese, P.W. Stephens, T. Vogt, R. Papoular, J. Solid State Chem. 120 (1995) 299–310.
[9] Belharouak, K. Amine, Electrochem. Commun. 7 (2005) 648–651.
[10] S. Kaoua, P. Gravereau, J.P. Chaminade, S. Pechev, S. Krimi, A. El Jazouli, Solid State Sci. 11 (2009) 628–634.
[11] S. Benmokhtar, A. El Jazouli, S. Krimi, J.P. Chaminade, P. Gravereau, M. Menetrier, D. De Wa al, Mater. Res. Bull. 42 (2007) 892–903.
[12] M. Kenza, E. Kristina, S. Ismael, T. Gustafsson, M. Mohammed, Electrochim. Acta 54 (2009) 5531.
[13] El Bouari, A. El Jazouli, Phosphorus Bull. 15 (2004) 136–139.
[14] S. Benmokhtar, A. El Jazouli, J.P. Chaminade, P. Gravereau, A. Wattiaux, L. Fournes, J.C. Grenier, Phosphorus Bull. 15 (2004) 140–142.
[15] B. Manoun, A. El Jazouli, P. Gravereau, J.P. Chaminade, F. Bourée, Powder Diff. 17 (4) (2002) 290–294.
[16] P. Blaha, K. Schwarz, G.K.H. Madsen, D. Kvasnicka, J. Luitz, WIEN2K, "An Augmented Plane Wave+Local Orbitals Program for Calculating Crystal Properties", Karlheinz Schwarz, Techn. Universitat, Wien, Austria, ISBN 3-9501031-1-2, 2001.
[17] J.P. Perdew, S. Burke, M. Ernzerhof, Phys. Rev. Lett. 77 (1996) 3865.
[18] E. Engel, S.H. Vosko, Phys. Rev. B 47 (1993) 13164.
[19] N.V. Smith, Phys. Rev. B 3 (1862) (1971).
[20] F. Wooten, Optical Properties of Solids, Academic Press, New York and London, 1972.
[21] B. Chakraborrty, W.E. Pickett, P.B. Allen, Phys. Rev. B 14 (1972) 3227.
[22] Ali Hussain Reshak, Xuean Chen, S. Auluck, I.V. Kityk, J. Chem. Phys. 129 (2008) 204111.
[23] Ali Hussain Reshak, I.V. Kityk, S. Auluck, J. Phys. Chem. B 114 (2010) 16705–16712;
Ali Hussain Reshak, S. Auluck, I.V. Kityk, Appl. Phys. A 91 (2008) 451–457;
Ali Hussain Reshak, J. Chem. Phys. 125 (2006) 034710;
Ali Hussain Reshak, J. Chem. Phys. 124 (2006) 104707;
Ali Hussain Reshak, Eur. Phys. J. B 47 (2005) 503–508;
Ali Hussain Reshak, S. Auluck, I.V. Kityk, J. Phys.: Condens. Matter 20 (2008) 145209;
Ali Hussain Reshak, Sushil Auluck, Phy. Rev. B 71 (2005) 155114;
Ali Hussain Reshak, Sushil Auluck, Physica B 358 (2005) 158–165.
[24] H. Tributsch, Z. Naturforsch. A 32A (1977) 972.
[25] S. Loughin, R.H. French, L.K. De Noyer, W.-Y. Ching, Y.-N. Xu, J. Phys. D: Appl. Phys 29 (1996) 1740.